Iran. J. Biotechnol. July 2022;20(3): e3110 DOI: 10.30498/ijb.2022.297534.3110

Research Article

Fabrication and Characterization of pcDNA3.1(+) Location within Chitosan/Nanoparticles Complexes for Enhanced Gene Delivery

Tohid Piri-Gharaghie[1], Abbas Doosti[2,*], Seyed Abbas Mirzaei[1,3]

[1]Department of Biology, Faculty of Basic Sciences, Shahrekord Branch, Islamic Azad University, Shahrekord, Iran
[2]Biotechnology Research Center, Shahrekord Branch, Islamic Azad University, Shahrekord, Iran
[3]Cellular and Molecular Research Center, Basic Health Sciences Institute, Shahrekord University of Medical Sciences, Shahrekord, Iran.

[*]*Corresponding author*: Abbas Doosti, Biotechnology Research Center, Shahrekord Branch, Islamic Azad University, Shahrekord, Iran, P.O. Box: 166, Shahrekord, Iran. Tel: +98- 3833361048, Fax: +98-3833361001, E-mail: Abbasdoosti@iaushk.ac.ir

Background: Chitosan nanoparticles (CSNP) are becoming a popular alternative for delivering nucleic acids to tissues for gene transfer (gene therapy). The size and morphology of these biodegradable nano-carriers are adjustable, and their positive charge allows them to interact strongly with negatively charged nucleic acids.

Objective: This study aimed to fabricate and characterize pcDNA3.1 (+) plasmid (pDNA) and CSNP complexes and determine the plasmid location in these vehicles.

Materials and Methods: The characteristics of the pDNA/CSNP complex after production were investigated by SEM, XRD, DLS, TGA, and FTIR**.** The capacity of CSNP to form complexes with pDNA was investigated by labeling free plasmids with the fluorescent intercalating dye OliGreen. The stability of pDNA/CSNP in the presence of chitosanase was evaluated. Surface-Enhanced Raman Spectroscopy (SERS) for pDNA localization was performed, and absorption rate in BALB/c mice was assessed by real-time PCR.

Results: The optimum pDNA/CSNP ratio for plasmid complex formation was established to be 1:2 (w.w) by measuring spectroscopy. At these optimum complex formation ratios, spectroscopy, and gel digest experiments, SERS indicated that a part of the pDNA was present on the complex outer surface. The findings of plasmid absorption in mouse thigh tissue by real-time PCR revealed that the rate of gene uptake was significantly greater at a dose of 1:2 (w.w) of pDNA/CSNP than in other groups ($P< 0.001$).

Conclusions: The findings of this study reveal exactly pDNA fits into polymer nanostructured delivery systems, allowing the formulation to be adjusted for selective distribution. This understanding will aid future research into the system's functioning in vitro and in vivo.

Keywords: Chitosan Nanoparticles, Gene Delivery, P-DNA, Vectors

1. Background

Gene therapy has been promoted as a revolutionary method of delivering and expressing genes in recent decades. However, the scientific community's mistrust following the tragic events of viral vectors has hindered medical adoption of this type of treatment (1). Consequently, all gene therapy clinical trials, particularly those utilizing viral vectors, were temporarily halted or confined to ex vivo studies due to safety reasons (2). As a result, current studies focus on improving nucleic acid delivery models or enhancing viral and non-viral vectors (3). Researchers' interest in non-viral gene transport

vehicles, direct injection of genetic material, and the use of plasmids based on lipids, polysaccharides, and polymeric materials have risen due to immunogenicity issues and the risk of viral vectors (4). Direct insertion of genetic material into tissues such as skin and muscle has been proven to be invasive for most people over the years (5). Due to their biocompatibility and ability to penetrate the interior of most target tissues, non-viral vectors, such as liposomes and polymer nanoparticles (NPs), do not have the difficulties that direct injection and viral vectors possess (6-7). Liposomes, polyethylene glycol, and chitosan (CS) are the most common non-viral cationic nanostructures that have been studied for their simplicity of usage and high transfer efficiency, amongst many other things (10).

On the other hand, polymeric NPs offer two benefits over liposomes: simplicity of manipulation, control of DNA diffusion patterns, and in vivo biological stability (8-9). The potential of CS to transfer genes as a biodegradable and biocompatible polymer was introduced in the early 1990s while seeking novel non-viral vehicles (11). CS has high cell uptake and transfers efficiency under physiological conditions, owing to its molecular mass, amount of acetylation, and quantity of varied primary amine groups (12). In addition to biocompatibility and biodegradation, CS/pDNA interactions are simple to make and do not shrink the extent of plasmids (14-13). CS may also be lyophilized, and CS in CS/pDNA complexes can successfully preserve pDNA from DNases (15). The primary issue with non-viral transmission techniques right now is their low transfection efficiency (16). Current research has utilized low molecular weight CS in gene delivery plasmids to increase transfection effectiveness (17). The capacity of nanostructures to prevent encapsulated pDNA from being degraded by nucleases has also been extensively established (18). The influence of nanostructures on the characteristics of encapsulated pDNA, on the other hand, is little characterized (19). The morphology of particle-ring interactions and the validation of pDNA encapsulation by NPs have been studied in current data. However, the position of pDNA in nanoparticle structures has not been investigated. (17-20). In advancing gene therapy, efficient manufacturing techniques necessitate a thorough analysis of polymeric materials before and after gene delivery. Because the biochemical characteristics of nanostructures might alter following nucleic acid interaction, a thorough knowledge of the therapeutic effectiveness of such linkages is necessary (10-21).

2. Objectives

Recently, many advances have been made in modifying polymer nanostructures as systems for improving drug delivery and gene therapy. However, the position of pDNA in pDNA-nanoparticle complexes is unknown. This analysis aimed to construct pDNA/CSNP complexes and explore the physicochemical characteristics of these complexes, including determining the relative location of pDNA in the complex.

3. Materials and Methods

3.1. Construction and Purification of Recombinant Plasmids: pDNA/gene

Recombinant plasmids of pDNA carrying the virulence gene (516bp) were extracted by using a plasmid extraction mini kit (FAVORGEN® recommended, Taiwan).

3.2. Preparation of pDNA/CSNP

3.2.1. Preparation of CS Solutions and Plasmid DNA Solutions

CS (100µg) was dissolved overnight in 1 mL of 0.5 % hydrochloric acid (w.v) using a rotary mixer. The diluted CS solutions were sterile filtered using a 0.2 mm syringe filter. The plasmid DNA solutions were diluted to a final concentration of 100 µg.mL with Na2SO4 solution (0.5 mmol.L).

3.2.2. Preparation of pDNA/CSNP

The diluted CS solutions were sterile filtered using a 0.2 mm syringe filter before being mixed with pDNA. At room temperature, 250 µL of sterile diluted CS solution was added to 250 µL of pDNA, pipetting up and down, and gently tapping the tubes to make pDNA/CSNP (1:1). In order to produce pDNA/CSNP (1:2), 500 µL of sterile diluted CS solution was pipetted into 250 µL of pDNA and gently tapped the tubes.

3.3. Characterization of the pDNA/CSNP

3.3.1. Particle Size, Zeta Potential, and Surface Morphology of the pDNA/CSNP

Dynamic light scattering (DLS) on Zetasizer was used

to measure the particle size of the NPs (Brookhaven Instruments Corp., USA). The surface morphology of NPs was observed by field scanning electron microscopy (FESEM) model MIRA3 (TESCAN, Czech Republic) and XRD model X' Pert Pro (Panalytical, Netherlands).

3.3.2. TGA and FTIR Assay

A thermal-gravimetric analyzer was used to evaluate the CS content of surface-modified NPs (BXT-DSC-TGA-1250, BAXIT, China). Purified pDNA/CSNP was deposited in an alumina crucible and scanned in TGA at a rate of 10 $C.min^{-1}$ under nitrogen flow starting at 40°C. The pDNA/CSNP were detected using Fourier transform infrared spectroscopy (FTIR, TENSOR II, BRUKER, Germany).

3.4. DNA Entrapment and Electrophoretic Mobility

1X OliGreen (OG) fluorescent nucleic acid stain (1X concentration in water, 25 µL) was introduced to compounds containing 4ng of pDNA and incubated at room temperature in a dark area for 5 minutes. Following incubation, distilled water was used to increase the total volume in the cuvette (1.5 mL) to 500µL. A BMG LABTECH's ultra-fast (UV.Visible) Luminescence Spectrophotometer (Ortenberg, Germany) was used to measure the relative fluorescence using 490 nm excitation and 520 nm emission wavelengths. Finally, 1:1 and 1:2 (w/w) pDNA and CSNP ratios were used to examine complexes.

Gel electrophoresis was used to measure the electrophoretic mobility of pDNA/CSNP complexes. 100 ng of pDNA (10 ng.µL) incomparable pDNA/CSNP ratios were combined with 4µL of loading buffer, loaded into agarose gels (0.8 % w.v), and run in TBE buffer at 6 $V.cm^{-1}$ for 40 minutes, followed by 15 minutes of SYBR Safe (Invitrogen) staining and visualization on a transilluminator.

3.5. Stability of the pDNA/CSNP

At 37 °C for 30 minutes, 1.35 µg of naked plasmid DNA and the pDNA/CSNP solution, including 1.35 µg of plasmid DNA, were treated using DNase I (1.0 U.mL). At 65 °C for 10 minutes, the process was halted by mixing 100 µL of termination supplies (400 mmol.L NaCl, 100 mmol.L EDTA, pH 8.0). Also, 16µL of chitosanase (0.2 U.mL) and 4.0 µL of lysozyme (0.2 U.mL) were introduced and incubated for 1 hour in a 37 °C heating block. 0.8% agarose gel electrophoresis was used to evaluate the stability of plasmid DNA.

3.6. Surface-Enhanced Raman Spectroscopy (SERS) for pDNA Localization

Silver NPs (SNP) with a diameter of 10 to 20 nm were obtained from Invitrogen for the SERS investigations (Invitrogen, USA). Under stirring for 2 hours over ice, the pDNA/CSNP complex suspension was combined in equal parts with the SNP colloidal solution. For Raman analysis, a few drops of the finished mixture were placed on a glass slide. At ambient temperature, Raman scattering experiments were conducted using a Horiba Jobin Yvon LabRam HR800 spectrometer with a charge-coupled detector and two grating systems: 600 and 1800 (lines.mm) and a 633 nm (1.96 eV) laser excitation.

3.7. Gene Delivery Analysis

In this investigation, 30 female BALB/c mice aged 6 to 8 weeks weighing 15–20g were employed. The mice were separated into three groups of 10. Animals have been injected, according to **Table 1**, through IM injections in both hind legs (100 µL of total volume per leg). The mice were boosted twice after the initial IM injection, using identical injection techniques on days 7 and 14. Seven days after the last dosage, the quadriceps muscle was collected from mice. The number of genes delivered in each group was then evaluated using real-time PCR.

Table 1. Grouping of mice in this study

Group number	Injection composition	dosage	Number of mice	Average weight of mice	Type of injection
1	pcDNA3.1(+)/gene	200 µL	10	18.7	IM
2	pcDNA3.1(+)/CSNP	200 µL (1:1)	10	18.2	IM
3	pcDNA3.1(+)/ CSNP	200 µL (1:2)	10	18.9	IM

3.8. Statistical Analysis

The mean difference between groups was the analysis of variance (ANOVA) statistical techniques in the Statistical Package for Social Sciences (SPSS, Inc., Chicago, IL, USA) version 16. The results were statistically significant at a level of $P<0.05$.

4. Results

4.1. Construction of Eukaryotic Expression Plasmids

A very safe plasmid (pDNA) was used to construct an optimal NPs structure. The constructed plasmid was then amplified in *E. coli* and analyzed on an agarose gel electrophoresis following extraction. The pDNA is represented band in **Figure 1A**.

4.2. Particle Size, Zeta Potential, and Surface Morphology of the pDNA/CSNP

CSNP and pDNA/CSNP, having spherical structures, have mean sizes of 25.93 ± 0.98 and 50.12 ± 0.48 nm, respectively (**Fig. 1B**). The size of the complexes was examined as a function of pDNA/CSNP ratios ranging from 0 (no DNA) to 1 (w.w), as illustrated in **Figure 1C.** The impact of complexing NPs with pDNA binding at various ratios resulted in particle sizes rising as the pDNA/CSNP ratio rose. For 1:1 and 1:2 (w.w) pDNA/CSNP complexes, all pDNA/CSNP complexes remained smaller than 150 nm in size. **Figure 1C** shows that the identical pDNA/ CSNP complexes were positively charged, with a zeta potential greater than 20 mV at all ratios investigated. The polydispersity index (PDI) is another important parameter that describes the width or spread of the particle size distribution. In general, If the polydispersity index is> 0.1, the cumulative fit error is> 0.001, or the resulting quality is poor, then data is considered suspicious, and further analysis is needed. Actually, the PDI value may vary from 0 to 1, where the colloidal particles with PDIs less than 0.1 implies monodisperse particles, and the values more than 0.1 may imply polydisperse particle size distributions (34). PDI of the CSNP and pDNA/CSNP were 0.095 ± 0.005 and 0.107 ± 0.024, respectively. The quality of the produced NPs is suitable and acceptable since the dispersion index is less than 0.1. Also, the PDIs less than 0.1 in the CSNP imply monodisperse particles, and the values of pDNA/CSNP that was more than 0.1 may imply polydisperse particle size distributions (34). Therefore, the type of single-phase or multi-phase produced NPs was determined using an XRD diagram. As a result of the XRD diagram, the maximum reflection at 30125, 32410, 39563, and 48357 degrees (**Fig. 2A**) was attributed to pDNA/CSNP, whereas angles of 29720 degrees (**Fig. 2B**) were attributed to CSNP. The XRD patterns reveal that all the CSNP samples with reflection at 29720 degrees are single phase in nature. pDNA/CSNP (1:1) and pDNA/CSNP (1:2) NPs showed multiphasic nature with multiple reflections. All the peaks of the pDNA/CSNP shift to the high angle side with increasing concentration (35). Due to the negative charge of pDNA, the CSNP (with a positive charge) is compressed toward the center when the concentration of pDNA in the solution approaches 1:1 (pDNA/ CSNP). In the TGA diagram, the start temperature of the thermal deterioration of CSNP was at 315 °C, and it entirely disintegrated at 400 °C, leaving just 4.5%. CSNP›s weight reduction was separated into two stages, the first of which was the water loss stage. CSNP lost a little weight (5%) at the onset of thermal deterioration, indicating that it contained around 5% free water. Thermal deterioration was the next stage. At 295 °C, CSNP began to disintegrate, and 34.7% of it remained at 800 °C. At 800 °C, the pDNA/CSNP (1:1) and pDNA/CSNP (1:2) remained 9.4% and 17.8%, respectively. In the initial, the mass ratios of CSNP to pDNA/CSNP (1:1) and pDNA/CSNP (1:2) were 50%, and 66.6 %, respectively. The mass ratios of CSNP to pDNA/CSNP (1:1) and pDNA/CSNP (1:2) were calculated to be 39.2% and 58.7%, respectively, based on the findings of thermal analysis, which are extremely near to the initial ratios.

FT-IR spectroscopy found a non-sharp characteristic peak (36), and a very strong broad peak has been detected at 2079 cm^{-1} and 3329 cm^{-1}. Because the CSNP used in this study was not entirely deacetylated, the peak at 2857 cm^{-1} shows the presence of an amide I band, whereas the peak at 1378 cm^{-1} suggests PO bending (**Fig. 3A**). In the pDNA/CSNP, absorption bands have been identified at 3329 cm^{-1}, 2928 cm^{-1}, 2858 cm^{-1}, 2079 cm^{-1}, and 1739 cm^{-1} (**Fig. 3B**). The waves' NH and OH stretching phases are responsible for the peaks seen at about 2928 –3329 cm^{-1} of pDNA/CSNP (37, 38). The asymmetrical CH bending in the mixtures is indicated by a peak produced at 2857 cm^{-1}. At 1742 cm^{-1}, the spectrum shows the development of imine interaction in pDNA and CSNP.

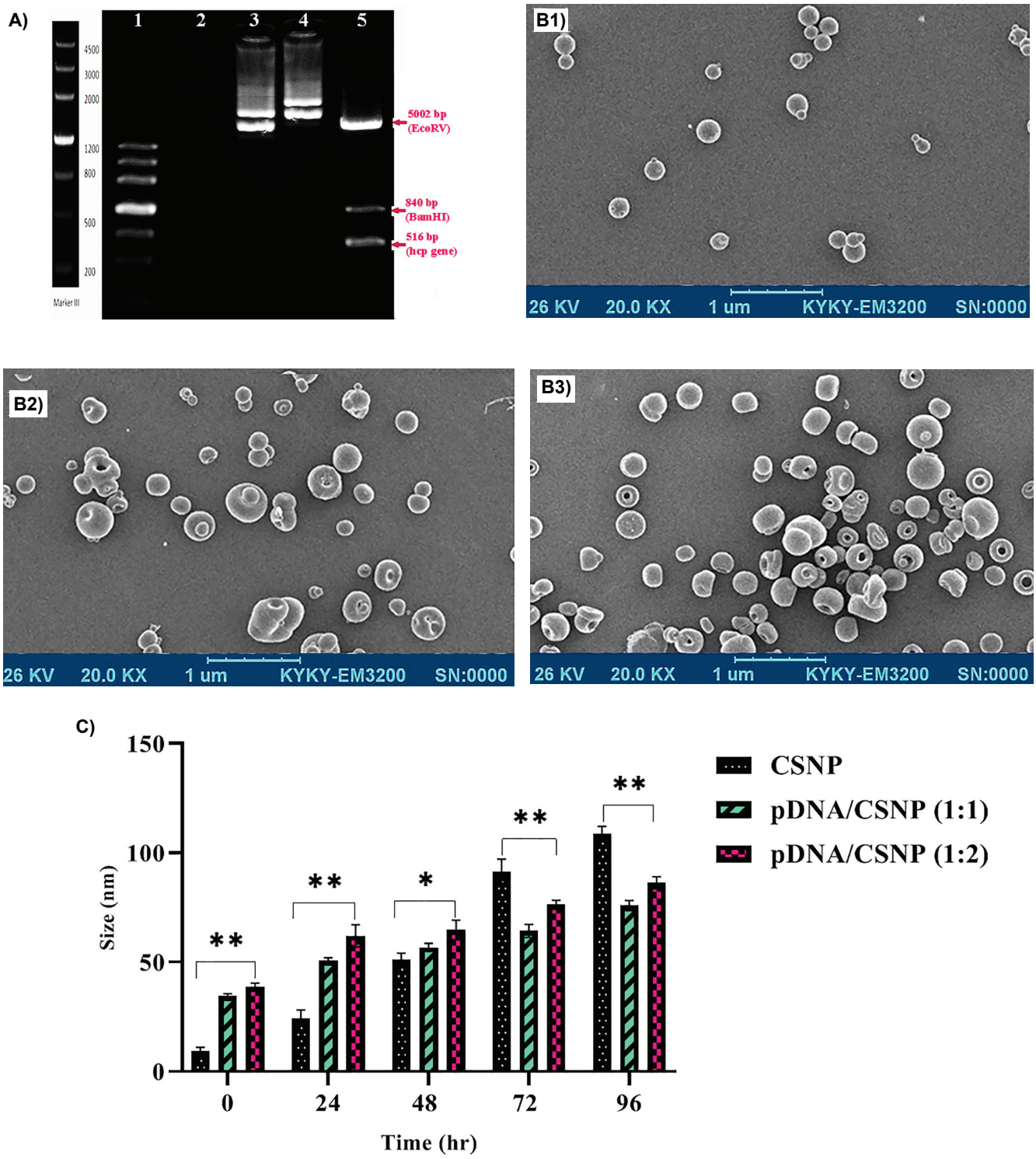

Figure 1. A) PCR reaction to validate pcDNA3.1(+) vector purity. Lane 1, DNA MarkerIII; Lane 2, Negative control; Lane3, Positive control (Free pDNA vector with 5482 bp band); Lane 4, pDNA-gene vector; Lane 5, Expected Size of Restriction enzymes and virulence gene. **B1)** CSNP, **B2)** pDNA/CSNP (1:1) and **B3)** pDNA/CSNP (1:2) having spherical structures. **C)** pDNA/CSNP complex size as a function of pDNA/CSNP ratios (n=3; mean standard error). The size of the pDNA/CSNP complexes was reduced as predicted when additional negatively charged pDNA was added. The presence of a negatively charged pDNA appears to prevent the aggregation of CSNPs. Also, the 1:1 ratio of pDNA/CSNP had the greatest effect on preventing size increase during the 96-hour period. *P<0.05; **P<0.01

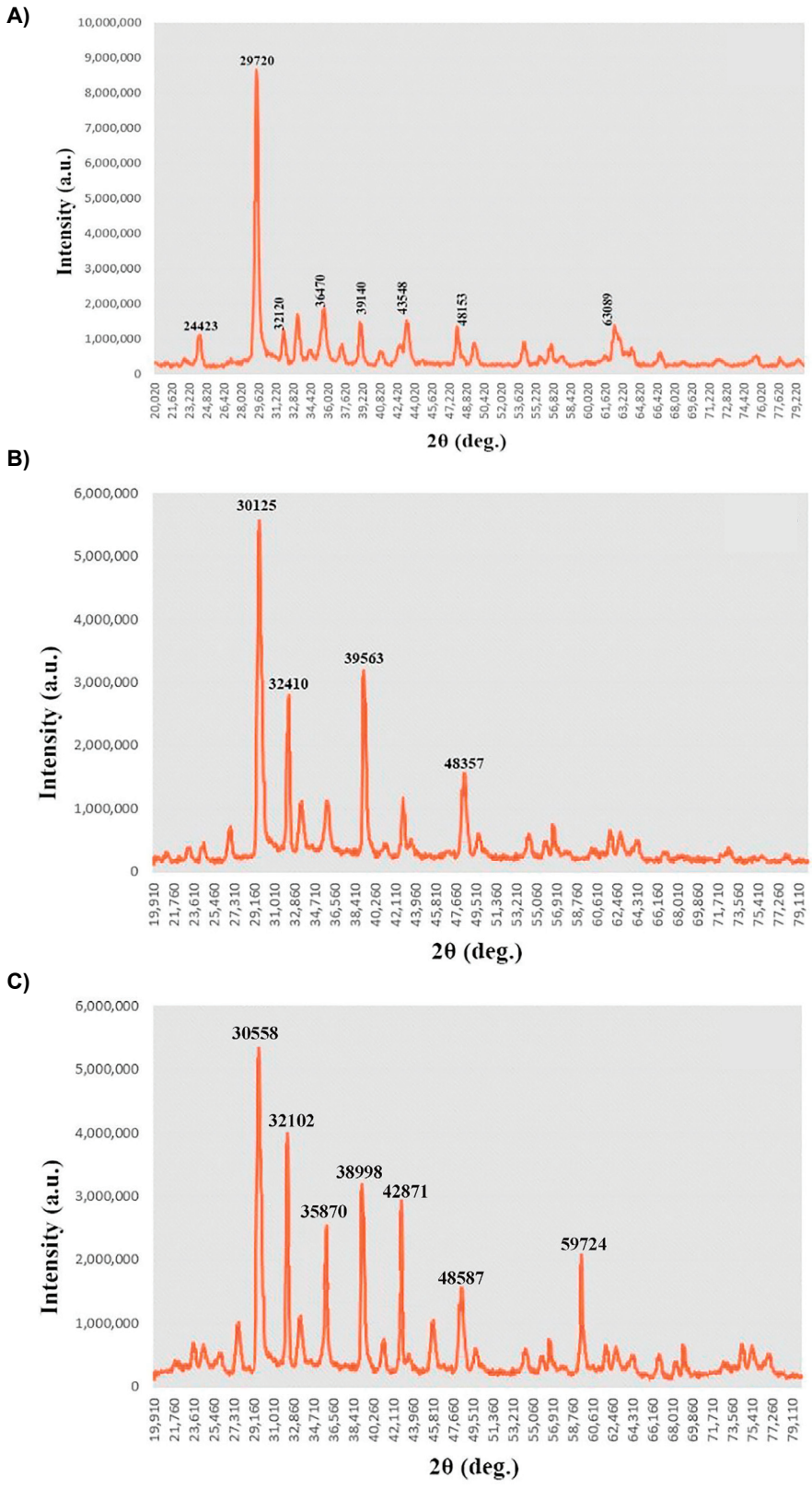

Figure 2. XRD pattern of the **A)** CSNP, **B)** pDNA/CSNP (1:1) and **C)** pDNA/CSNP (1:2) structures. The presence of pDNA/CSNP is shown by multiple prominent peaks in Figures **B** and **C**.

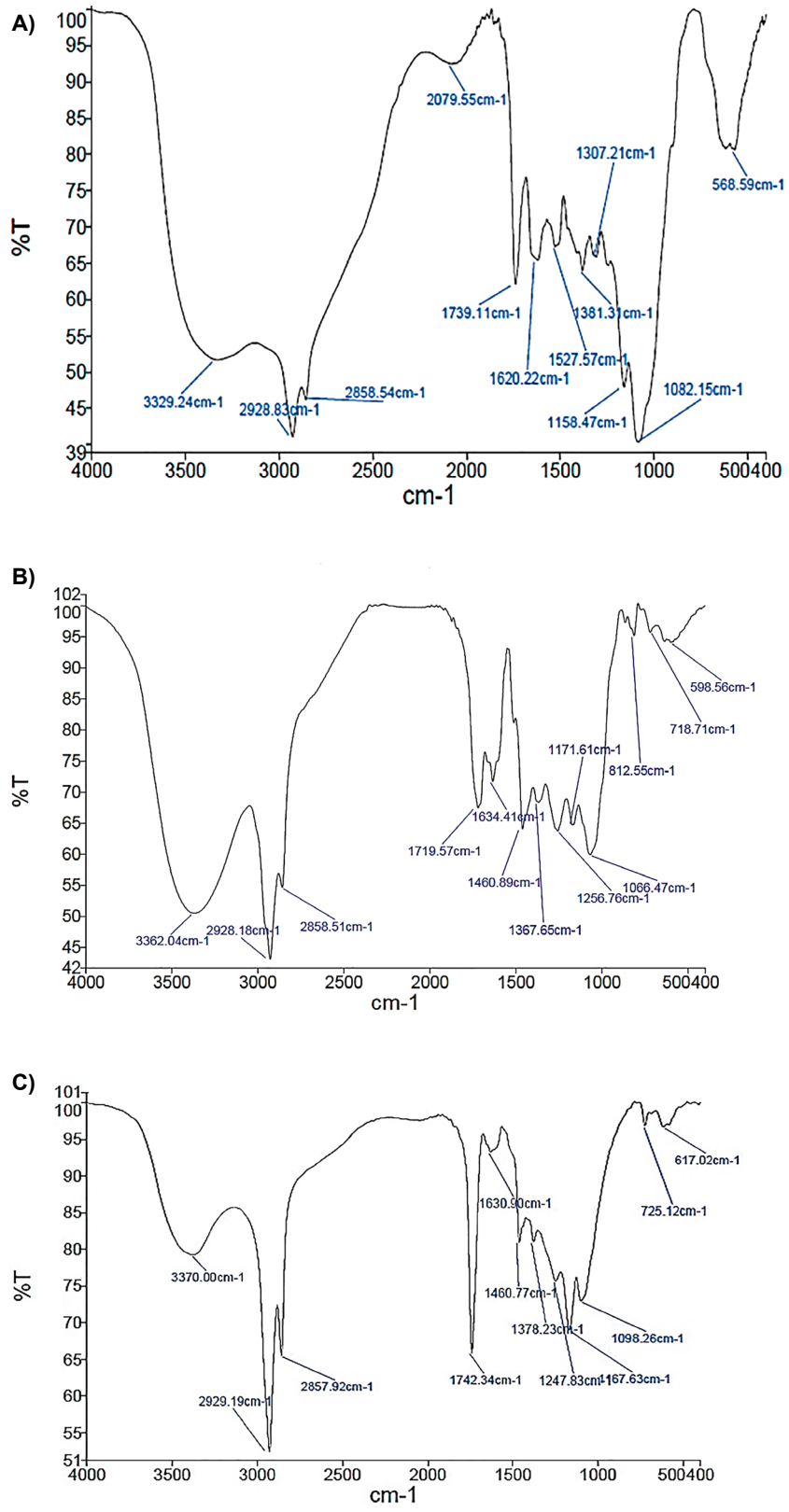

Figure 3. FTIR spectra of **A)** pDNA/CSNP (1:1), **B)** pDNA/CSNP (1:2), **C)** CSNP. The 3329 cm^{-1} and 3362 cm^{-1} peaks in Figures **A** and **B** belong to the O-H group. The appearance of this peak in pDNA/CSNP demonstrates proper pDNA loading in the CSNP (36, 39).

The carbonyl group (C=O) has a large dipole moment and thus an intense stretching vibration whose peak generally appears from 1900 to 1600. Also, the carbonyl carbon in the C=O bond has a large positive partial charge (39). Therefore, due to the negative charge in pDNA, a large tension is created between the positive charge of the carbonyl group (C=O) and the negative charge of pDNA and forms a strong bond in this region.

4.3. DNA Entrapment and Electrophoretic Mobility Studies

The OliGreen nucleic acid stain's comparative fluorescence indicates whether the DNA in the experiment is free or partially encapsulated. The sample containing solely free plasmid in water has the highest fluorescence. The reduction in fluorescence shows that pDNA has become complex to the extent where DNA dye interaction and fluorescence are no longer possible. Compared to free pDNA, a pDNA/CSNP ratio of 1:2 results in a 79.73% reduction in absorption spectra. The optimal ratio for protecting and delivering the whole DNA load is when all pDNA is completely absorbed (**Fig. 4A**). In lane 2 of the electrophoresis,

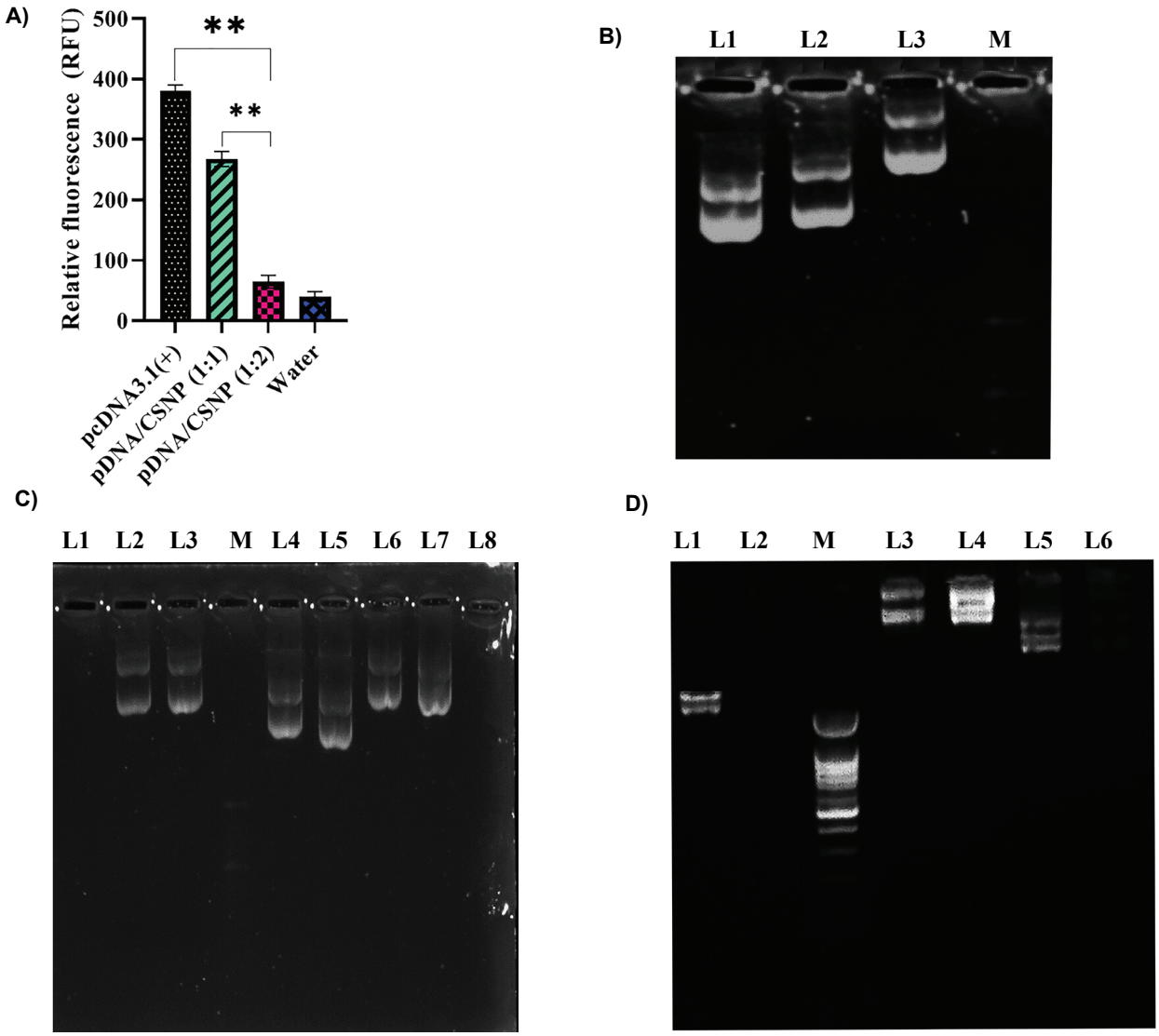

Figure 4. Gel analysis of complex formation and degradation. **A)** The number of NPs in each interaction determines the relative fluorescence of pDNA in each sample. Free pDNA has the most fluorescence. Fluorescence intensities decrease when the pDNA/CSNP ratio decreases (1:2) (n = 5; mean ± standard error; *P>0.05, **P>0.01).
B) Complexes formed at various ratios: lane 1= pDNA; lane 2= 1:1 ratio of pDNA/CSNP; lane 3= 1:2 ratio of pDNA/CSNP lane 4: 1kb ladder. **C)** after nuclease digestion using DNase I and **D)** Enzymic mixture (treated with chitosanase and lysozyme)

plasmid bands are observed in complexes, suggesting the existence of free pDNA in the investigated sample at a 1:1 pDNA/CSNP ratio, comparable to the bands observed in lane 1, which contain exclusively free pDNA. Following lane 3 of pDNA/CSNP combinations of ratio 1:2, no free pDNA band is observed, suggesting the full complex formation of all free pDNA (**Fig. 4B**).

4.4. CS Enhanced Stability of the pDNA

Gel electrophoresis shows the destruction of free pDNA after treatment with DNase I, with no bands evident save a weak band of high mobility close to the bottom of the concept (**Fig. 4C,** lane 4). The smearing pattern in lane 5 indicates that part of the pDNA in the combination was accessible for digest since pieces of varied sizes and mobility are evident compared to the undigested plasmids. Gel electrophoresis of digestion of free pDNA with this enzyme mixture in this system reveals no visible pDNA bands, indicating plasmid degradation (**Fig. 4D,** lane 2). When comparing lanes 4 and 5, it is clear that a 1:2 ratio of pDNA/CSNP is released from compounds after treatment with the enzyme combination, suggesting that the complex can shield pDNA from enzymatic destruction. In a 1:2 ratio of pDNA/CSNP, the encapsulation was protected against pDNA degradation by DNase I and chitosanase, but only slightly in a 1:1 ratio of pDNA/CSNP. The results showed that encapsulating 1:2 pDNA in CS protected the DNA from DNase I degradation.

4.5. Raman Spectroscopy Analysis

The lower peaks of **Figure 5** depict the typical Raman spectra of the pDNA/CSNP, which is typical of polymeric materials (with the highest peak characteristics correlating to the CH stretching modes of 734.19 cm^{-1}). For the concentration measurement of the polymeric CSNP related to pDNA, the 493 cm^{-1} peaks (rCH2) were used as a standard band. pDNA could be detected by very faint peaks superimposed on the polymeric spectra (40). As illustrated in **Figure 5**, silver NPs (SNPs) were coated onto the interfaces of the pDNA/CSNPs interactions, resulting in a significant increase in the pDNA output (Upper peak). The typical 721 cm^{-1} peaks ascribed to adenine are apparent, as in Raman and silver-based SERS investigations into DNA (41). The significant SERS impact produced via SNPs located on the surface of the pDNA/CSNP compounds was also exploited to get relative pDNA concentration information relative to the polymeric CSNPs as their concentration of a substance was changed in the following pDNA/CSNP ratios: 1:1 and 1:2. It is evident that when the pDNA/CSNP ratio drops, the percentages between the 721 cm^{-1} (pDNA) and 493 cm^{-1} (CSNP) peaks employ a standard declining pattern. As a result,

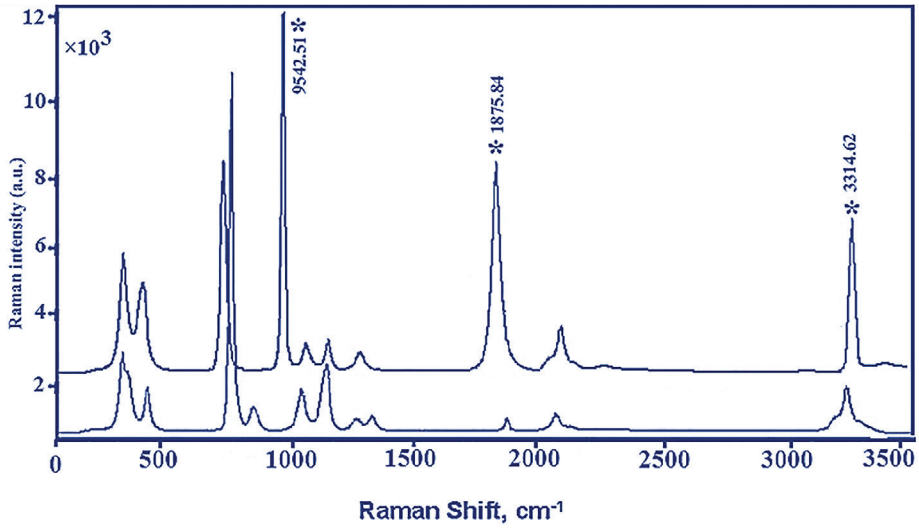

Figure 5. Typical Raman spectrum of the pDNA/CSNP complexes. Bottom line: SERS spectrum of the 1:2 ratio of pDNA/CSNP complexes coated with silver nanoparticles (SNPs). The high scattering peaks matching to pDNA can be seen, and as the signal was primarily gathered owing to the SERS effect caused by the SNPs, it can be assumed that the DNA is mostly present in the structure of the CSNP.

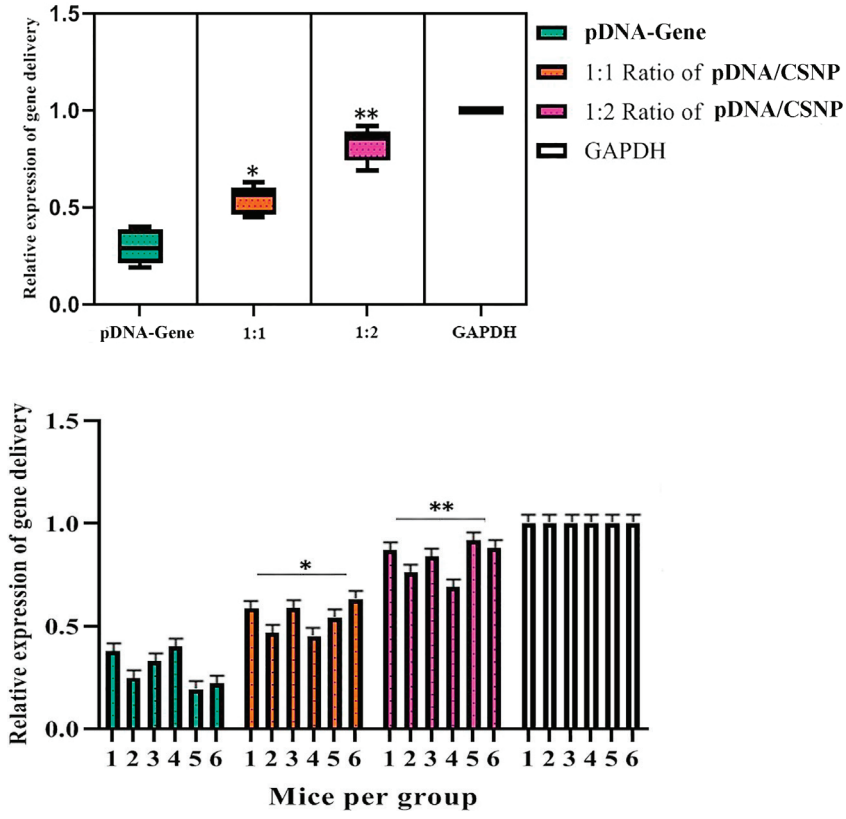

Figure 6. Virulence gene delivery increased significantly in groups with CSNP doses. According to the group's results, the mean expression of group 3 [pDNA/CSNP (1:2)] was significantly different from group 1 (pDNA) at the level of **P<0.001, and significantly different from group 2 [pDNA/CSNP (1:1)] at the level of *P<0.01. The GAPDH reference gene was used to normalize all of the data.

the CSNP covers of the pDNA compounds interface alter according to their respective concentrations.

4.6. CSNP Enhanced Gene Delivery

A real-time PCR study of the virulance gene was conducted to confirm gene delivery in animal tissue. We found that the expression of pDNA was increased successfully in group 3 (pDNA/CSNP 1:2). In contrast, such effects were not observed in group 1 with free pDNA and group 2 (pDNA/CSNP 1:1) (**Fig. 6**). Furthermore, plasmid vector activity in group 2 was much greater than in group 1 (free vector). These findings show that CSNP might play a role in increasing gene delivery to tissues.

5. Discussion

In this study, by comparing the relative fluorescence of products treated pDNA/CSNP interactions (1:2 ratio) to a purity water sample, the conjugation of all pDNA was demonstrated, indicating that no free pDNA is available. Because no free vector bands were evident in interactions with pDNA ratios lesser than 1:1, the absence of electrophoretic mobility of the pDNA in the complicated form significantly indicates total encapsulation. These results suggest that the fluorescence marking method and the electrophoresis mobility approach, both straightforwardly perform, have a reasonable correlation (22, 23). Following DNase and enzyme cocktails treatment, Gel electrophoresis indicated that CSNP interactions protect pDNA against enzymatic breakdown (24, 25). The nanoparticle component of the complexes is degraded by chitosanase/lysozyme digesting, which frees the pDNA. According to gel digestion assays, free pDNA cannot tolerate frequent interactions with the chitosanase/lysozyme mix and is destroyed. The existence of undamaged pDNA in the 1:2 complex sample indicates that the CSNPs can protect pDNA from enzyme degradation, which is critical for effective gene delivery in vivo. To determine the degree of free pDNA degradation,

DNase I was introduced to free pDNA as a baseline (28, 29, 42).

The nuclease-treated structures had low electrophoretic mobility, suggesting that part of the pDNA must be accessible to the inserted enzyme inside the combination. Because the interaction protects the pDNA within it against enzymatic degradation, this implies that the broken DNA resides on the complex's periphery. These results are consistent with Fielden *et al*. (26) and Zhang *et al*. (27). Although traditional Raman analysis of the compounds failed to reveal DNA patterns within the NP complex (28), silver-based SERS showed substantially increased DNA peaks and confirmed the presence of pDNA strands in the complexes' insides. This dual approach to interface research of polymeric CSNPs complex with distinct biological processes might be beneficial for investigating their morphological characteristics and tracking either in vitro or in vivo as they communicate with local tissues and cells (29, 30, 42, 43-46). The transport of biological agents into cells via nanoparticle platforms and the releasing of bioactive medicines from polymeric nano surfaces might both benefit from such methods (31, 47). Encapsulating pDNA into CSNP is a potential method for gene delivery (32, 33). The injection of CSNP to pDNA improves structural integrity, making them a good candidate for gene delivery systems that may be utilized to encapsulate other plasmids. When combined with a CSNP polymer-based gene delivery vector, this method guarantees that the positive charge of the CSNP NPs is decreased, making them more biodegradable with better safety and efficacy. Furthermore, this improves the delivery system's effectiveness, as seen by the real-time PCR assay. The position of pDNA within polymeric nanostructured delivery systems will be clarified, allowing formulations to be optimized for selective distribution with little breakdown. Novel factors will be essential to the implementation, approval, and medical delivery of these medicines. More research is necessary to confirm if the in vitro and in vivo transport and expression of pDNA in this variant of the pDNA/CSNP complex correlates with the various biochemical characteristics performed in this work.

Acknowledgements

The authors would like to thank the staff members of Biotechnology Research Center of Islamic Azad University of Shahrekord Branch in Iran.

References

1. Goswami R, Subramanian G, Silayeva L, Newkirk I, Doctor D, Chawla K, Chattopadhyay S, Chandra D, Chilukuri N, Betapudi V. Gene therapy leaves a vicious cycle. *Front Oncol*. 2019;**9**:297. doi: 10.3389/fonc.2019.00297
2. Baghdan E, Pinnapireddy SR, Strehlow B, Engelhardt KH, Schäfer J, Bakowsky U. Lipid coated chitosan-DNA nanoparticles for enhanced gene delivery. *Int J Pharm*. 2018;**535**(1-2):473-479. doi: 10.1016/j.ijpharm.2017.11.045
3. Bono N, Ponti F, Mantovani D, Candiani G. Non-viral in vitro gene delivery: it is now time to set the bar! *Pharmaceutics*. 2020;**12**(2):183. doi: 10.3390/pharmaceutics12020183
4. Thomas M, Klibanov AM. Non-viral gene therapy: polycation-mediated DNA delivery. *Appl Microbiol Biotechnol*. 2003;**62**(1):27-34. doi: 10.1007/s00253-003-1321-8
5. Ahlén G, Frelin L, Höolmstrm F, Smetham G, Augustyn S, Sällberg M. A targeted controlled force injection of genetic material in vivo. *Mol Ther Methods Clin Dev.* 2016;**3**:16016. doi: 10.1038/mtm.2016.16
6. Patil S, Gao YG, Lin X, Li Y, Dang K, Tian Y, Zhang WJ, Jiang SF, Qadir A, Qian AR. The development of functional non-viral vectors for gene delivery. *Int J Mol Sci.* 2019;**20**(21):5491. doi: 10.3390/ijms20215491
7. Mohammadinejad R, Dehshahri A, Madamsetty VS, Zahmatkeshan M, Tavakol S, Makvandi P, Khorsandi D, Pardakhty A, Ashrafizadeh M, Afshar EG, Zarrabi A. In vivo gene delivery mediated by non-viral vectors for cancer therapy. *J Control Release*. 2020;**325**:249-275. doi: 10.1016/j.jconrel.2020.06.038
8. Ninan G, Jose J, Abubacker Z. Preparation and characterization of gelatin extracted from the skins of rohu (Labeo rohita) and common carp (Cyprinus carpio). *J Food Process Preserv*. 2011;**35**(2):143-162. doi: 10.1111/j.1745-4549.2009.00467
9. Rizvi SA, Saleh AM. Applications of nanoparticle systems in drug delivery technology. *SPJ***.** 2018;**26**(1):64-70. doi: 10.1016/j.jsps.2017.10.012
10. Rai R, Alwani S, Badea I. Polymeric nanoparticles in gene therapy: New avenues of design and optimization for delivery applications. *Polymers*. 2019;**11**(4):745. doi: 10.3390/polym11040745
11. Santos-Carballal B, Fernández Fernández E, Goycoolea FM. Chitosan in non-viral gene delivery: Role of structure, characterization methods, and insights in cancer and rare diseases therapies. *Polymers*. 2018;**10**(4):444. doi: 10.3390/polym10040444
12. Lavertu M, Methot S, Tran-Khanh N, Buschmann MD. High efficiency gene transfer using chitosan/DNA nanoparticles with specific combinations of molecular weight and degree of deacetylation. *Biomaterials*. 2006;**27**(27):4815-4824. doi: 10.1016/j.biomaterials.2006.04.029
13. Wu Y, Rashidpour A, Almajano MP, Metón I. Chitosan-based drug delivery system: Applications in fish biotechnology. *Polymers*. 2020;**12**(5):1177. doi: 10.3390/polym12051177
14. Deng RH, Qiu B, Zhou PH. Chitosan/hyaluronic acid/plasmid-DNA nanoparticles encoding interleukin-1 receptor antagonist attenuate inflammation in synoviocytes induced by interleukin-1 beta. *J Mater Sci Mater Med*. 2018;**29**(10):1-10. doi: 10.1007/s10856-018-6160-3
15. Patil S, Gao YG, Lin X, Li Y, Dang K, Tian Y, Zhang WJ, Jiang SF, Qadir A, Qian AR. The development of functional non-viral

vectors for gene delivery. *Int J Mol Sci*. 2019;**20**(21):5491. doi: 10.3390/ijms20215491
16. Cao Y, Tan YF, Wong YS, Liew MW, Venkatraman S. Recent advances in chitosan-based carriers for gene delivery. *Mar drugs*. 2019;**17**(6):381. doi: 10.3390/md17060381
17. Morachis JM, Mahmoud EA, Sankaranarayanan J, Almutairi A. Triggered rapid degradation of nanoparticles for gene delivery. *J Drug Deliv***.** 2012;**20**:12. doi:10.1155/2012/291219
18. Jo A, Ringel-Scaia VM, McDaniel DK, Thomas CA, Zhang R, Riffle JS, Allen IC, Davis RM. Fabrication and characterization of PLGA nanoparticles encapsulating large CRISPR–Cas9 plasmid. *J nanobiotechnology*. 2020;**18**(1):1-4. doi: 10.1186/s12951-019-0564-1
19. Xiao Y, Shi K, Qu Y, Chu B, Qian Z. Engineering nanoparticles for targeted delivery of nucleic acid therapeutics in tumor. *Mol Ther Methods Clin Dev*. 2019;**12**:1-8. doi: 10.1016/j.omtm.2018.09.002
20. Suwatronnakorn M, Issaravanich S, Palanuvej C, Ruangrungsi N. Standardization of Leonurus sibiricus L. aerial part and capillary electrophoresis quantitative analysis of its leonurine content. *J Adv Pharm Technol Res*. 2021;**12**(3):291. doi: 10.4103/japtr.JAPTR_243_21
21. Bordelon H, Biris AS, Sabliov CM, Todd Monroe W. Characterization of plasmid DNA location within chitosan/PLGA/pDNA nanoparticle complexes designed for gene delivery. *J Nanomaterials*. 2011;**20**:11. doi: 10.1155/2011/952060
22. McCall J, Smith JJ, Marquardt KN, Knight KR, Bane H, Barber A, DeLong RK. ZnO nanoparticles protect RNA from degradation better than DNA. *Nanomaterials*. 2017;**7**(11):378. doi: 10.3390/nano7110378
23. Baghani A, Yousefi M, Safdari H, Teimourpour R, Gholoobi A, Meshkat Z. Designing and construction a DNA vaccine encoding the fusion fragment of cfp10 and Ag85A immunodominant genes of Mycobacterium tuberculosis. *Arch Med Lab Sci*. 2017;**2**(4). doi: 10.22037/amls.v2i4.17185
24. Harman JL, Loes AN, Warren GD, Heaphy MC, Lampi KJ, Harms MJ. Evolution of multifunctionality through a pleiotropic substitution in the innate immune protein S100A9. *Elife*. 2020;**9**:e54100. doi: 10.7554/eLife.54100
25. Garikipati VN, Verma SK, Cheng Z, Liang D, Truongcao MM, Cimini M, Yue Y, Huang G, Wang C, Benedict C, Tang Y. Circular RNA CircFndc3b modulates cardiac repair after myocardial infarction via FUS/VEGF-A axis. *Nat Commun*. 2019;**10**(1):1-4. doi: 10.1038/s41467-019-11777-7
26. Fielden J, Wiseman K, Torrecilla I, Li S, Hume S, Chiang SC, Ruggiano A, Singh AN, Freire R, Hassanieh S, Domingo E. TEX264 coordinates p97-and SPRTN-mediated resolution of topoisomerase 1-DNA adducts. *Nat Commun*. 2020;**11**(1):1-6. doi: 10.1038/s41467-020-15000-w
27. Zhang Y, Zhang J, Chen Y, Luo B, Yuan Y, Huang F, Yang T, Yu F, Liu J, Liu B, Song Z. The ORF8 protein of SARS-CoV-2 mediates immune evasion through potently downregulating MHC-I. *BioRxiv*. 2020;**1**. doi: 10.1101/2020.05.24.111823
28. Calderon I, Guerrini L, Alvarez-Puebla RA. Targets and Tools: Nucleic Acids for Surface-Enhanced Raman Spectroscopy. *Biosensors*. 2021;**11**(7):230. doi: 10.3390/bios11070230
29. Bashir S, Hina M, Iqbal J, Rajpar AH, Mujtaba MA, Alghamdi NA, Wageh S, Ramesh K, Ramesh S. Fundamental concepts of hydrogels: Synthesis, properties, and their applications. *Polymers*. 2020;**12**(11):2702. doi: 10.3390/polym12112702
30. Detsi A, Kavetsou E, Kostopoulou I, Pitterou I, Pontillo AR, Tzani A, Christodoulou P, Siliachli A, Zoumpoulakis P. Nanosystems for the encapsulation of natural products: The case of chitosan biopolymer as a matrix. *Pharmaceutics*. 2020;**12**(7):669. doi: 10.3390/pharmaceutics12070669
31. Neerooa BN, Ooi LT, Shameli K, Dahlan NA, Islam JM, Pushpamalar J, Teow SY. Development of polymer-assisted nanoparticles and Nanoparticles for cancer therapy: An update. *Gels*. 2021;**7**(2):60. doi: 10.3390/gels7020060
32. Valente JF, Pereira P, Sousa A, Queiroz JA, Sousa F. Effect of Plasmid DNA Size on Chitosan or Polyethyleneimine Polyplexes Formulation. *Polymers*. 2021;**13**(5):793. doi: 10.3390/polym13050793
33. Chehelgerdi M, Doosti A. Effect of the cagW-based gene vaccine on the immunologic properties of BALB/c mouse: an efficient candidate for Helicobacter pylori DNA vaccine. *J nanobiotechnology*. 2020;**18**(1):1-6. doi: 10.1186/s12951-020-00618-1
34. Raval, Nidhi, *et al.* "Importance of physicochemical characterization of nanoparticles in pharmaceutical product development." *Bf Drug Delivery*. 2019;369-400. doi:10.1016/B978-0-12-817909-3.00010-8
35. Malik K, Das D, Mondal D, Chattopadhyay D, Deb AK, Bandyopadhyay S, Banerjee A. Sb concentration dependent structural and resistive properties of polycrystalline Bi-Sb alloys. *Int J Appl Phys.* 2012;**112**(8):083706. doi:10.1063/1.4759137
36. Zhuang J, Li M, Pu Y, Ragauskas AJ, Yoo CG. Observation of potential contaminants in processed biomass using fourier transform infrared spectroscopy. *Appl Sci.* 2020;**10**(12):4345. doi:10.3390/app10124345
37. Van Beijnen AJ, Nolte RJ, Naaktgeboren AJ, Zwikker JW, Drenth W, Hezemans AM. Helical configuration of poly (iminomethylenes). Synthesis and CD spectra of polymers derived from optically active isocyanides. *Macromolecules*. 1983;**16**(11):1679-1689. doi:10.1021/ma00245a001
38. Kumar S, Koh J. Physiochemical, optical and biological activity of chitosan-chromone derivative for biomedical applications. *Int J Mol Sci.* 2012;**13**(5):6102-6116. doi:10.3390/ijms13056102
39. Smith BC. The carbonyl group, part I: introduction. 2017.
40. O'connor T, Mansy S, Bina M, McMillin DR, Bruck MA, Tobias RS. The pH-dependent structure of calf thymus DNA studied by Raman spectroscopy. *Biophys Chem.* 1982;**15**(1):53-64. doi:10.1016/0301-4622(82)87016-6
41. Feng F, Zhi G, Jia HS, Cheng L, Tian YT, Li XJ. SERS detection of low-concentration adenine by a patterned silver structure immersion plated on a silicon nanoporous pillar array. *Nanotechnology*. 2009;**20**(29):295501. doi: 10.1088/0957-4484/20/29/295501/meta
42. Ghorbani-Dalini S, Kargar M, Doosti A, Abbasi P, Sarshar M. Molecular epidemiology of ESBL genes and multi-drug resistance in diarrheagenic *Escherichia coli* strains isolated from adults in Iran. *Iran. J. Pharm. Sci.* 2015;**14**(4):1257-1262.
43. Ansari H, Tahmasebi-Birgani M, Bijanzadeh M, Doosti A, Kargar M. Study of the immunogenicity of outer membrane protein A (ompA) gene from Acinetobacter baumannii as DNA vaccine candidate *in vivo*. *Iran. J. Basic Med. Sci*. 2019;**22**(6):669-675 doi:10.22038/ijbms.2019.30799.7427.
44. Beiranvand S, Doosti A, Mirzaei SA. Putative novel B-cell

vaccine candidates identified by reverse vaccinology and genomics approaches to control Acinetobacter baumannii serotypes. *Infect. Genet. Evol*. 2021:105138. doi:10.1016/j.meegid.2021.105138

45. Piri Gharaghie T, Sadat Shandiz SA, Beiranvand S. Evaluation of silver nanoparticles effects on bla-per1 gene expression for biofilm formation in isolates of antibiotic-resistant Acientobacter Bumanni by real time PCR method. *Cel. and Mol. Res. (Iranian Journal of Biology)*. 2020;**16**.
46. Piri Gharaghie T, Doosti A, Mirzaei SA. Prevalence and antibiotic resistance pattern of Acinetobacter spp. infections in Shahrekord medical centers. *Dev. Biol.* 2021;**13**(4). doi: jdb.iau-tnb.ac.ir/article_686587.html
47. Doosti A, Pourabbas M, Arshi A, Chehelgerdi M, Kabiri H. TEM and SHV genes in Klebsiella pneumoniae isolated from cockroaches and their antimicrobial resistance pattern. Osong Public Health Res Perspect. 2015;6(1):3-8.